Korean J. Chem. Eng., 33(9), 2582-2588 (2016)
DOI: 10.1007/s11814-016-0113-7

pISSN: 0256-1115
eISSN: 1975-7220

Fe/N/C catalysts systhesized using graphene aerogel for electrocatalytic oxygen reduction reaction in an acidic condition

Chi-Woo Roh and Hyunjoo Lee†

Department of Chemical and Biomolecular Engineering, Korea Advanced Institute of Science and Technology, Daejeon 34141, Korea

(*Received 9 February 2016 • accepted 22 April 2016*)

Abstract−Graphene aerogel was modified with polyaniline and Fe precursors to produce Fe/N/C catalysts for electrocatalytic oxygen reduction reaction in the acidic condition. The graphene aerogel was produced by a simple hydrothermal treatment of graphene oxide dispersion with a high surface area. Aniline was polymerized with the graphene aerogel powder, and the pyrolysis of the resulting material with $FeCl_3$ produced Fe/N/C catalyst. The loading amount on the electrode and the catalyst ink concentration was carefully selected to avoid the mass transfer limitation inside the catalyst layer. The pyrolysis temperature affected the states of nitrogen sites on the catalyst; the sample prepared at 900 °C presented the highest mass activity. The sulfur was also doped with various amounts of $FeSO_4$ with enhanced mass activity of up to 2.1 mA/mg at 0.8 V in 0.5 M H_2SO_4 solution. Its durability was also tested by repeating cyclic voltammetry in a range of 0.6-1.1 V 5000 cycles. This graphene-aerogel-based carbon catalysts showed improved activity and durability for the oxygen reduction reaction in the acidic condition.

Keywords: Fe/N/C, Polyaniline, Oxygen Reduction Reaction, Acidic Condition, Graphene Aerogel

INTRODUCTION

The oxygen reduction reaction (ORR) is a key reaction for recent energy devices, especially for fuel cells. ORR kinetics is well-known to be sluggish, so the development of good cathode catalysts for fuel cells is important [1]. In proton exchange membrane fuel cell (PEMFC), platinum (Pt) or Pt-based catalysts have been extensively studied. However, high cost and scarcity of Pt hinder the commercialization of the PEMFC. To overcome these problems, many researchers have investigated the alternative non-Pt catalysts including non-Pt noble metals, non-noble metal alloys, and carbon catalysts [2]. Since Jasinsky found that cobalt phthalocyanine can be used as ORR catalyst [3], metal-nitrogen-carbon (Me/N/C) systems have been actively studied for the ORR catalysts [4-8]. Although it is being debated whether the metal is an active site or not in these catalysts [5,7-12], Fe-containing carbon catalysts show superior activities in an acidic condition among various Me/N/C catalysts [6,13].

For the Fe/N/C catalysts, various kinds of carbon materials, including carbon black [6], carbon nanotubes [14], mesoporous carbon [15], have been applied. Graphene with high surface area, good electrical and thermal conductivity, and high mechanical strength has been actively studied for various applications such as supercapacitors [16-18], batteries [19,20], sensors [21,22], and it is also considered as a promising material for carbon catalysts [23]. However, graphene sheets stack easily due to π-π interaction [24,25] with rather poor ORR activities [26]. To prevent graphene sheets from being stacked, 3-dimensional (3-D) graphene structures have been developed [27-31]. Zhao et al. fabricated 3-D graphene foams by using silica as hard templates, but the template had to be removed by toxic HF later [32]. Xu et al. synthesized graphene aerogel (GA) by a simple hydrothermal treatment from graphene oxide dispersion without any template [33]. The oxygen-containing groups on the graphene oxide were reduced and π-π interaction between the sheets were partially restored, producing 3-D framework. This graphene aerogel has high surface area, good electrical conductivity, and facile processibility with a potential as a good carbon catalyst. The nitrogen can be doped into the carbon catalysts using NH_3 [34], dicyandiamide [26], or polyaniline [6] as N-sources in the Fe/N/C catalysts. Polyaniline (PANI) can make direct coordination between nitrogen in the polymer chain and metal ions [34]. Fe ions would be uniformly dispersed on N-sites in the PANI [35]. Furthermore, the structural similarity of PANI containing aromatic structures with graphene might facilitates N-doping into the carbon framework [36].

In this work, we synthesized Fe-containing N-doped graphene aerogel catalyst for the ORR in the acidic condition. The graphene aerogel would insure large surface area and pore volume with potentially more active sites containing dopants. With *in situ* polymerization, polyaniline could be deposited on the graphene aerogel substrate, and pyrolysis of PANI-GA in the presence of Fe ions would make Fe/N-doped graphene structure with enhanced ORR activity. To improve the activity further, S was additionally doped. The durability of Fe/N/GA catalyst was also tested.

EXPERIMENTAL

1. Materials

Graphite (Bay Carbon), H_2SO_4 (≥95.0 wt%, Samchun), H_3PO_4

†To whom correspondence should be addressed.
E-mail: azhyun@kaist.ac.kr

(≥85.0 wt%, Fluka), $KMnO_4$ (≥99.0 wt%, Sigma-Aldrich), H_2O_2 (≥28.0 wt%, Duksan), HCl (36.0 wt%, Samchun), anhydrous ethanol (≥99.9 wt%, Samchun), $HClO_4$ (70 wt%, Sigma-Aldrich), aniline (≥99.5 wt%, Sigma-Aldrich), ammonium peroxydisulfate (APS, ≥98.0 wt%, Sigma-Aldrich), $FeCl_3$ (97 wt%, Sigma-Aldrich), $FeSO_4 \cdot 7H_2O$ (≥99.0 wt%, Sigma-Aldrich), Nafion® perfluorinated resin solution (5 wt%, Sigma-Aldrich), and isopropyl alcohol (IPA, ≥99.7 wt%, JUNSEI) were purchased and used without further purification. Deionized water (18.3 MΩ·cm) was prepared by Human Power II+ Scholar (Human Corporation).

2. Synthesis of Graphene Aerogel (GA)

Graphene oxide (GO) was prepared by the modified Hummer's method [37]. In a typical procedure, graphite (0.5 g) was dispersed in a mixture of the concentrated H_2SO_4 (60 ml) and the concentrated H_3PO_4 (13.33 ml). $KMnO_4$ (3.0 g) was added slowly under vigorous stirring while the temperature was kept under 10 °C in an ice bath. The solution was kept stirred at 50 °C for additional 12 h. The solution was poured into 100 ml of ice and 0.5 ml of H_2O_2 was added. The obtained graphite oxide was washed with 10 wt% HCl solution, deionized water, and ethanol in sequence by centrifugation at 4,000 rpm for 10 min, and a series of process is repeated four times. Then the graphite oxide is dispersed in deionized water and sonicated for more than 3 h before use. Graphene aerogel (GA) was synthesized following the previously reported recipe by heating 10 ml of GO dispersion solution (2 mg/ml) in a Teflon-lined stainless steel vessel at 180 °C for 12 h and freeze-drying the resulting materials [33].

3. Synthesis of Fe/N/C Catalysts Using Polyaniline (PANI)-coated GA

The GA (30 mg) was dispersed in 100 ml of 1 M $HClO_4$ and 6 mmol of aniline monomer was dissolved in the solution. The solution was stirred well for 1 h and cooled under 5 °C in an ice bath. Then, 2 mmol of APS and 6 mmol of $FeCl_3$ were added and the solution was stirred for 6 h while the temperature was maintained under 5 °C. The solution was filtered and the solid residue was re-dispersed in 20 ml of aqueous solution where 6 mmol of $FeCl_3$ was dissolved, and left overnight. The resulting solution was freeze-dried. The obtained powder was pyrolyzed at 800 °C, 900 °C, or 1,000 °C for 1 h, followed by the acid treatment at 0.5 M H_2SO_4 for 8 h. Then, the powder was pyrolyzed again at the same temperature for 3 h. The obtained powders were named as PANI-GA-800, PANI-GA-900, and PANI-GA-1000, where the number denotes the calcination temperature. For comparison, PANI-GO was also prepared by the same method as PANI-GA-900 by polymerizing aniline on GO instead of GA.

The S content was also controlled. The synthetic procedure was the same as PANI-GA-900 except that $FeCl_3$ and $FeSO_4$ were used together when the Fe salts were added again after filtration. PANI-GA-0.05S, PANI-GA-0.1S, PANI-GA-0.25S or PANI-GA-1.0S were prepared. The numbers 0.05, 0.1, 0.25, and 1.0 denote the fraction of $FeSO_4$ when the total mole number of Fe salts ($FeCl_3$+$FeSO_4$) was 6 mmol.

4. Characterizations

The carbon-based catalysts were observed by field emission scanning electron microscopy (FE-SEM, Magellan 400). The surface properties were measured by X-ray photoelectron spectroscopy (XPS, K-alpha). Binding energies were calculated using the maximum intensity of the C 1s signal at 284.8 eV as a reference. Nitrogen adsorption-desorption isotherm was measured by BET surface area analyzer (ASAP 2020).

5. Electrochemical Measurements

The measurements were conducted using a conventional three-electrode cell with a glassy carbon electrode (GCE, 0.2475 cm^2), a Pt wire, and Ag/AgCl/3 M NaCl as a working, counter and reference electrode, respectively. All potentials were calibrated to a reversible hydrogen electrode (RHE) potential, which was measured by performing hydrogen evolution and oxidation reactions in a H_2-purged electrolyte using a rotating Pt electrode prior to each measurement. The mixture of Nafion solution and the catalyst with a ratio of 4 μl of the Nafion solution per 1 mg of the catalysts was dispersed into the mixture of IPA and deionized water with a volumetric ratio of 3 : 1 by ultra-sonication for 20 min. Various concentrations of the catalyst ink (10 mg/ml, 5 mg/ml, or 2 mg/ml) were prepared and tested. The amount of doped-carbon catalyst deposited on the GCE was also varied as 60, 200, 300, 600, 800, 1,000, or 1,500 μg/cm^2. Linear sweep voltammetry (LSV) was conducted on a rotating disk electrode (RDE) in 0.5 M H_2SO_4 solution from 1.1 V to 0.05 V with a scan rate of 10 mV/s. The ORR curves were obtained by subtracting capacitance measured in Ar-saturated 0.5 M H_2SO_4 without rotating from linear sweep voltammogram measured in O_2-saturated 0.5 M H_2SO_4 with 1,600 rpm. Accelerated degradation test (ADT) was conducted by repeating cyclic voltammetry (CV) in the range of 0.6-1.1 V with a scan rate of 100 mV/s for 5,000 cycles.

RESULTS AND DISCUSSION

The graphene aerogel (GA) was prepared by a simple hydrothermal reduction of graphene oxides dispersed in aqueous solution, and its SEM image is shown in Fig. 1(a). The GA has 3-dimensional crumbled structure. The GA powders were mixed with aniline monomer solution, then the anilines were polymerized to form polyaniline (PANI) on the GA support. $FeCl_3$ were added to the PANI-GA sample, and the resulting materials were freeze-dried and pyrolyzed. Fig. 1(b) shows SEM image of the PANI-GA when the sample was pyrolyzed at 900 °C. The carbon structure showed little difference from the GA. However, nitrogen adsorption-desorption isotherms in Fig. 1(c) indicate that surface area increased significantly from 421 m^2/g to 1,218 m^2/g. The PANI treatment produced much micropores. To confirm the effect of aerogel structure, we also performed the PANI treatment on graphene oxide (PANI-GO) following the same synthetic procedure. The PANI-GO also had a surface area similar to the PANI-GA-900. But when the carbon catalysts were used for the oxygen reduction reaction in the acidic condition, the PANI-GO exhibited much poorer activity than the PANI-GA-900 as shown in Fig. 1(d). The pore volumes were 0.50, 0.42, and 0.52 cm^3/g for GA, PANI-GO, and PANI-GA-900, respectively. Although the surface area is similar for the PANI-GO and PANI-GA-900, the pore volume is much larger for the PANI-GA-900 and it has more mesopores as indicated by hysteresis in the P/P_0 range of 0.5-1.0, which makes the mass transfer much easier.

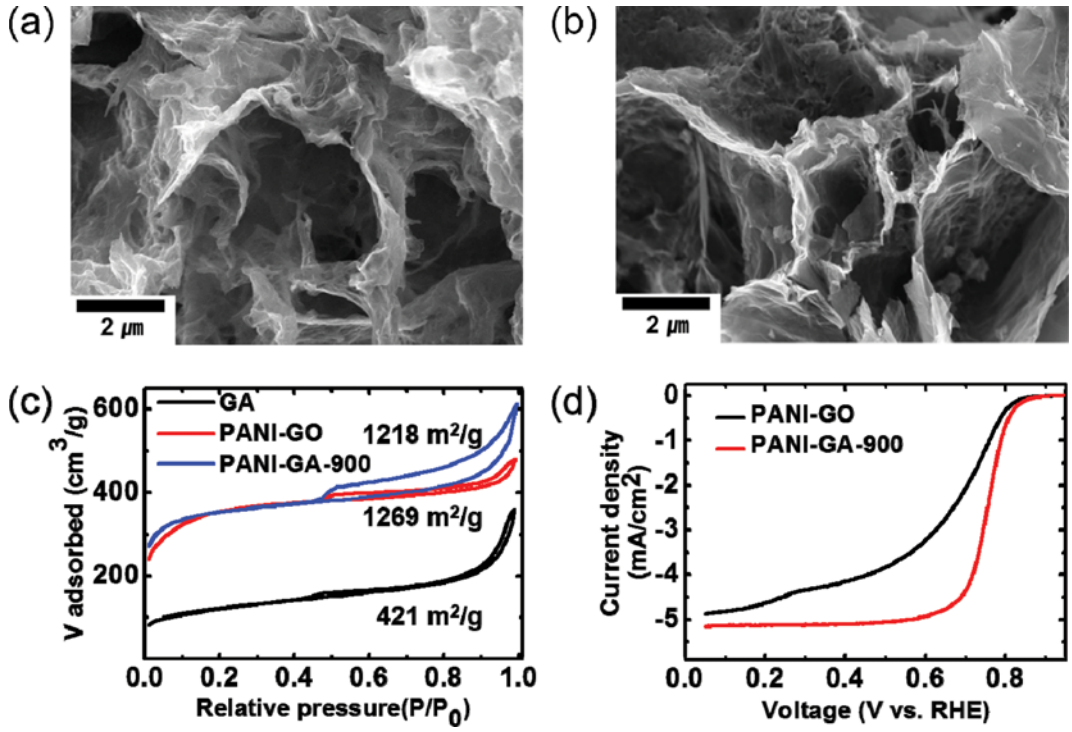

Fig. 1. SEM images of (a) GA and (b) PANI-GA-900. (c) Nitrogen adsorption-desorption isotherm curves for GA, PANI-GO and PANI-GA-900. (d) Linear sweep voltammetry results for PANI-GO and PANI-GA-900; the loading amount was 600 μg/cm^2, the catalyst ink concentration was 10 mg/ml, the rotation speed of the electrode was 1,600 rpm, and the scan rate was 10 mV/s in O_2-saturated 0.5 M H_2SO_4 electrolyte.

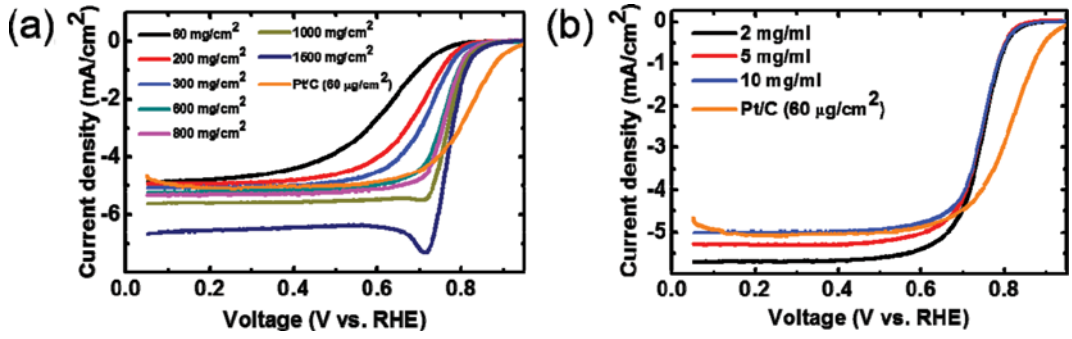

Fig. 2. Linear sweep voltammetry results for the electrodes deposited with (a) the different loading amounts of the PANI-GA-900 with an ink concentration of 10 mg/ml and (b) the different ink concentrations of the PANI-GA-900 with a loading amount of 600 μg/cm^2. The rotation speed of the electrode was 1,600 rpm, and the scan rate was 10 mV/s in O_2-saturated 0.5 M H_2SO_4 electrolyte.

The electrocatalytic activity for the ORR was tested for the PANI-GA-900 sample. Linear sweep voltammetry (LSV) was conducted on a rotating disk electrode (RDE) to evaluate the effects of the catalyst loading amount and the catalyst ink concentration on the RDE. Fig. 2(a) shows that the limiting current density becomes larger as the loading amount increases from 60 μg/cm^2 to 1,500 μg/cm^2. When the loading amount was larger than 800 μg/cm^2, the limiting current density was even larger than commercial Pt/C and a negative peak was observed at ~0.7 V. The RDE voltammetry assumes a thin catalyst layer with no mass transfer resistance inside the catalyst layer. The diffusion-limiting current density of the Pt/C catalyst would be the maximum value at the given reaction condition without the resistance inside the catalyst layer. The heavy loading of the catalyst would make the catalyst layer on the electrode thicker. It is known that the ORR on Fe/N/C catalysts in the acidic condition follows 2+2 electron reactions [13]; (1) the oxygen provided to the electrode is reduced to H_2O_2 ($O_2+2H^++2e^-\rightarrow H_2O_2$), then (2) the H_2O_2 moves to another active site and undergoes further reduction to H_2O ($H_2O_2+2H^++2e^-\rightarrow 2H_2O$) [11]. The reactant or intermediate species of O_2 and H_2O_2 might reside within the thick catalyst layer during the RDE voltammetry, resulting in the diffusion-limiting current density larger than the Pt/C catalyst. The peak at ~0.7 V is estimated as a reduction peak of H_2O_2 to H_2O. The concentration of the catalyst ink also affected the diffusion-limiting current density. Fig. 2(b) shows that the current density increased as the ink concentration decreased. When

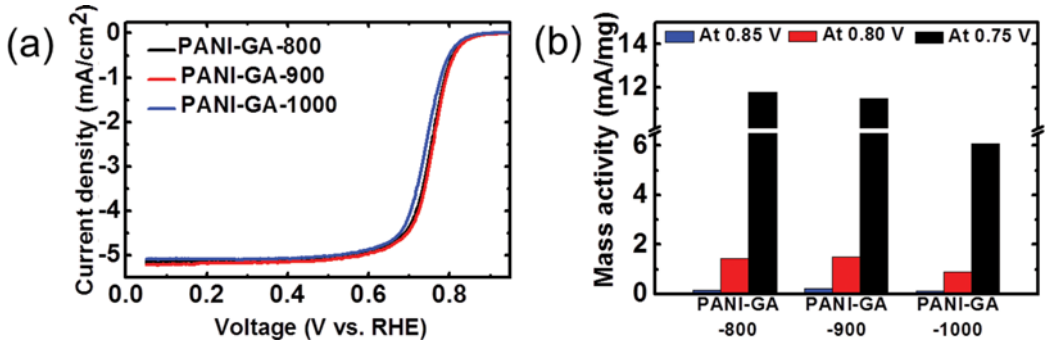

Fig. 3. (a) Linear sweep voltammetry results, and (b) mass activities at various voltages (vs. RHE) for PANI-GA-800, PANI-GA-900, and PANI-GA-1000; the loading amount was 600 μg/cm^2, the catalyst ink concentration was 10 mg/ml, the rotation speed of the electrode was 1,600 rpm, and the scan rate was 10 mV/s in O_2-saturated 0.5 M H_2SO_4 electrolyte.

the ink concentration was 10 mg/ml, the limiting current density was similar to that of the Pt/C catalyst. But as the ink concentration decreased, the limiting current density increased. The dilute ink possibly makes the contact between the powders more loose, with more space inside the catalyst film layer. Then O_2 or H_2O_2 would reside within the space longer, with larger limiting current density. To evaluate the electrocatalytic activity of the GA-based carbon catalysts properly, the loading amount of 600 μg/cm^2 and the ink concentration of 10 mg/ml were used to fabricate the working electrode.

The synthetic conditions of pyrolysis temperature and additional dopants affected the ORR activities of the PANI-GA-based catalysts. The effect of pyrolysis temperature was evaluated. Three different temperatures of 800, 900, 1,000 °C were compared. Fig. 3 shows the ORR activities for the samples prepared at various pyrolysis temperatures. When the onset potentials with a current density of 0.1 mA/cm^2 were measured, the potential was 0.849 V for PANI-GA-800, 0.856 V for PANI-GA-900, and 0.843 V for PANI-GA-1000, respectively. The sample prepared at 900 °C showed the lowest overpotential. SEM images for the three samples showed no difference.

XPS spectra of N1s orbital were measured for the three catalysts as shown in Fig. 4. The N peaks were deconvoluted to pyridinic (398.5 eV), pyrrolic (400.1 eV), graphitic (401.0 eV), and oxidized N (>402.0 eV), then each percentage was estimated as shown in Table 1. The pyrrolic peak exists only at PANI-GA-800 and the peak was not observed at the other samples. The pyridinic peak was significantly reduced for PANI-GA-1000. As the pyrolysis temperature increased, the pyrrolic peak disappeared above 900 °C and the pyridinic peak decreased from 18.1 at% at 800 °C to 15.8 at% at 900 °C then 4.5 at% at 1,000 °C. Choi et al. reported that turnover frequencies (TOF) on each site decrease in the order of pyridinic>graphitic>>pyrrolic N-site [38]. The amount of pyridinic N-sites would be the most important and the amount of graphitic N-sites would also play a role for the ORR. The ORR activity of PANI-GA-900 was

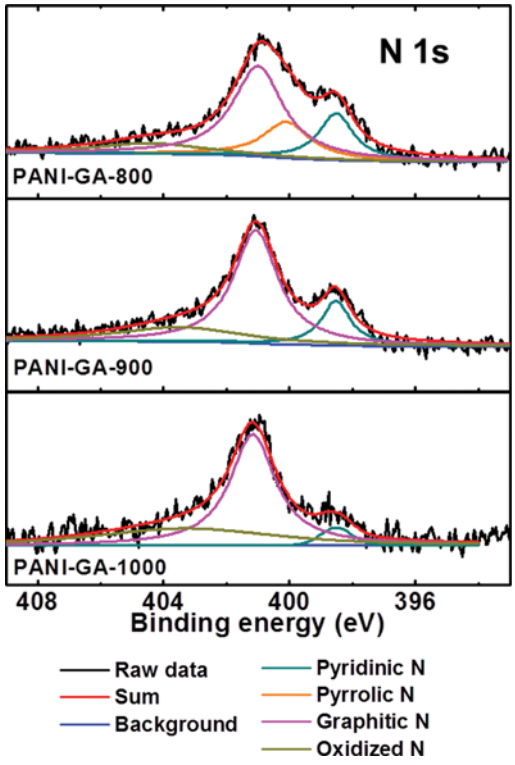

Fig. 4. XPS spectra for N 1s of PANI-GA-800, PANI-GA-900, and PANI-GA-1000.

the highest because the sample prepared at 900 °C had the highest proportion for the sum of pyridinic N sites and graphitic N-sites.

Sulfur was additionally doped into the GA-based catalyst by replacing a portion of $FeCl_3$, which was added after the PANI polymerization, into $FeSO_4$. Co-doping N and S into the carbon catalyst can enhance the ORR activity significantly [39]. It is known that

Table 1. The percentages of N species estimated from XPS analysis for the carbon catalysts prepared at various pyrolysis temperatures

at%	Pyridinic N	Pyrrolic N	Graphitic N	Oxidized N
PANI-GA-800	18.1	18.7	50.4	12.8
PANI-GA-900	15.8	-	61.6	22.6
PANI-GA-1000	4.5	-	63.2	32.3

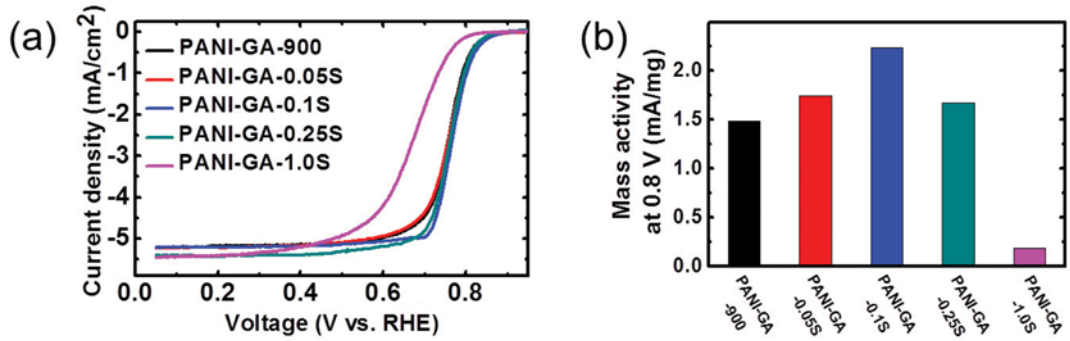

Fig. 5. (a) Linear sweep voltammetry results, and (d) mass activities at 0.8 V (vs. RHE) of S-doped PANI-GA catalysts the loading amount was 600 μg/cm^2, the catalyst ink concentration was 10 mg/ml, the rotation speed of the electrode was 1,600 rpm, and the scan rate was 10 mV/s in O_2-saturated 0.5 M H_2SO_4 electrolyte. The numbers at PANI-GA-'xx'S indicate the fraction of $FeSO_4$ replacing $FeCl_3$, which was added after the PANI polymerization. All the samples were pyrolyzed at 900 °C.

when S is additionally doped, a spin density of circumjacent carbon increases, which makes the binding strength of the oxygen species weakened [39,40]. Even in the absence of $FeSO_4$, a small amount of S existed in PANI-GA-900 because APS added during the PANI polymerization as an initiator provided sulfur. The atomic S percentages estimated from XPS were 0.33, 1.42, 1.49 and 1.65 at% for PANI-GA-900, PANI-GA-0.05S, PANI-GA-0.1S, and PANI-GA-0.25S. Fig. 5 shows the activity for the ORR when various amounts of $FeSO_4$ were added. The onset potential estimated at a current density of 0.1 mA/cm^2 was 0.856 V, 0.862 V, 0.864 V, 0.850 V, and 0.805 V for PANI-GA-900, PANI-GA-0.05S, PANI-GA-0.1S, PANI-GA-0.25S, and PANI-GA-1.0S, respectively. The overpotential was the lowest for the PANI-GA-0.1S sample. The same sample showed the highest mass activity when the activity was estimated at 0.8 V.

XPS spectra of S 2p orbitals were measured as shown in Fig. 6. The oxidized S and FeS existed additionally. The fraction of each species is listed in Table 2. When $FeSO_4$ was added, the S content increased and the fraction of oxidized S decreased significantly, with the enhanced ORR activity. However, when the fraction of $FeSO_4$ was higher than 0.25, the activity diminished due to the formation of extra species of FeS. Additionally, excessive $FeSO_4$ might also oxidize the carbon structure with less ORR activity.

Linear sweep voltammetry was conducted with PANI-GA-0.1S at several rotating speeds and plotted in Fig. 7. The number of electrons transferred per an O_2 molecule during the ORR can be calculated with Koutecky-Levich (K-L) equation:

$$\frac{1}{I} = \frac{1}{0.62nF\, C_{O_2} D_{O_2}^{2/3} \nu^{-1/6} \omega^{1/2}} + \frac{1}{nF\, kC_{O_2}}$$

where n is the number of electrons transferred per one O_2, F is

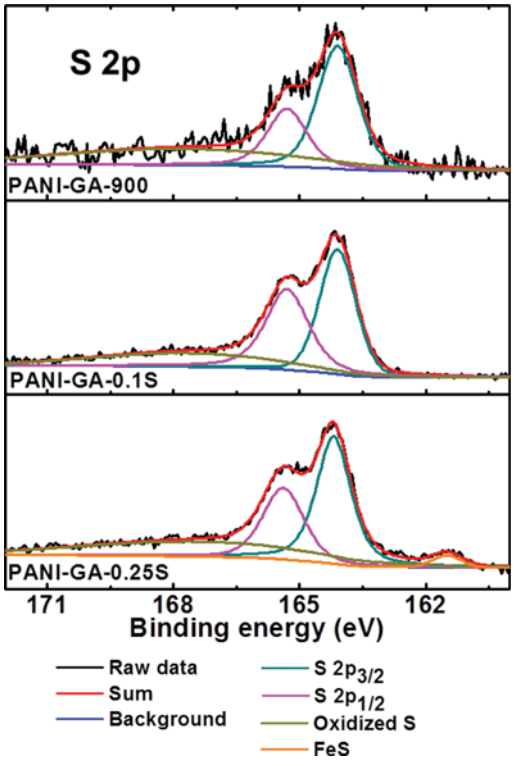

Fig. 6. XPS spectra for S 2p of PANI-GA-0.05S, PANI-GA-0.1S, and PANI-GA-0.25S.

Faraday constant (96,485 C/mol), C_{O_2} is the concentration of dissolved O_2 (1.3×10^{-6} mol/cm^2), D_{O_2} is the diffusion coefficient of dis-

Table 2. The percentages of N and S species estimated from XPS analysis for S-doped carbon catalysts

at%	N			S		
	Pyridinic N	Graphitic N	Oxidized N	S 2p	Oxidized S	FeS
PANI-GA-900	15.8	61.6	22.6	68.2	31.8	-
PANI-GA-0.05S	16.3	68.1	15.6	81.0	19.0	-
PANI-GA-0.1S	15.2	65.8	19.0	78.5	21.5	-
PANI-GA-0.25S	10.8	58.2	31.0	70.1	27.2	2.7

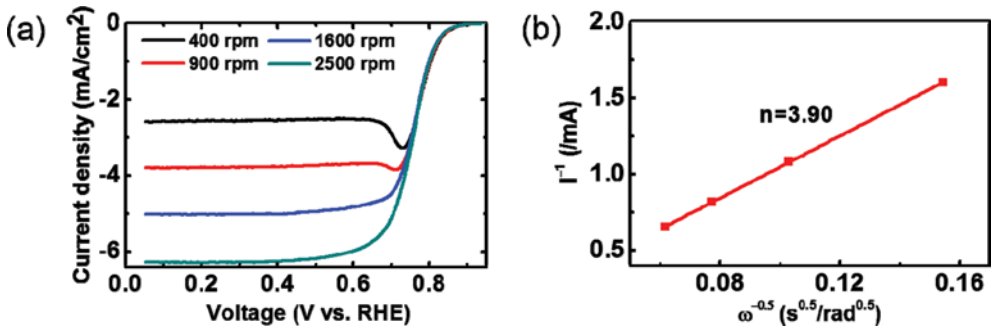

Fig. 7. (a) Linear sweep voltammetry results at several rotating speeds for PANI-GA-0.1S; the loading amount was 600 μg/cm^2, the catalyst ink concentration was 10 mg/ml and the scan rate was 10 mV/s in O_2-saturated 0.5 M H_2SO_4 electrolyte. (b) Koutecky-Levich plot at 0.5 V (vs. RHE).

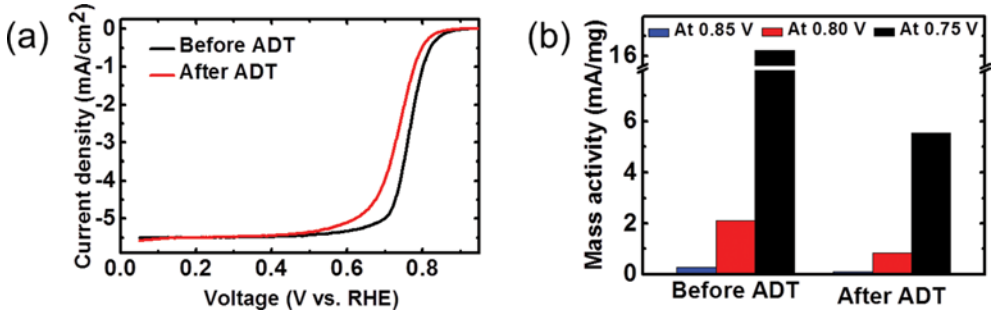

Fig. 8. (a) Linear sweep voltammetry results, and (b) mass activities at various voltages (vs. RHE) for PANI-GA-0.1S before and after ADT. The ADT was conducted for 5000 cycles in a range of 0.6-1.1 V with a scan rate of 100 mV/s in O_2-saturated 0.5 M H_2SO_4 solution.

solved O_2 (1.5×10^{-5} mol/s), ν is the kinematic viscosity of solution (0.01 cm^2/s), ω is the rotation speed, and k is the rate constant for the ORR. According to the K-L equation, n was calculated as 3.90 for PANI-GA-0.1S at 0.5 V (vs. RHE). The n value was estimated as 3.70 for PANI-GA-900, and 3.41 for PANI-GO, respectively. PANI-GA-0.1S catalyst reduced the oxygen more efficiently for the ORR comparing to the other carbon catalysts.

For the PANI-GA-0.1S that showed the best ORR activity, its stability was tested by performing an accelerated durability test (ADT). The ADT was performed by repeating cyclic voltammetry in a range of 0.6-1.1 V with a scan rate of 100 mV/s in O_2-saturated 0.5 M H_2SO_4 aqueous solution. Fig. 8 shows the linear sweep voltammogram before and after the ADT, and the changes in mass activity at 0.75, 0.80, and 0.85 V. The onset potential was negatively shifted; the potential with a current density of 0.1 mA/cm^2 changed from 0.863 V to 0.839 V, and the mass activity at 0.8 V decreased to 40% from 2.10 mA/mg to 0.83 mA/mg. The carbon-based catalyst can react with water, generating CO and CO_2 [41]. Table 3 shows the change in N-sites before and after the ADT. The fraction of pyridinic N decreased from 15.8% to 5.5%, and this degradation in active sites would be responsible for the decrease in the ORR activity. This durability result is compared with other carbon catalysts from literatures. Table 4 shows the ORR activity before and after the ADT for various carbon catalysts. The comparison clearly confirmed that this GA-based carbon catalyst has a good activity and durability for the ORR in an acidic condition.

Table 3. The change in the percentages of various N-species estimated from XPS analysis on PANI-GA-0.1S before and after ADT

at%	Pyridinic N	Graphitic N	Oxidized N
Before ADT	15.8	61.6	22.6
After ADT	5.5	82.0	12.5

Table 4. Comparison of the ORR activity and durability in the acidic condition

Catalysts	Electrolyte (conc)	Initial mass activity (mA/mg)	ADT condition	Final mass activity (mA/mg)	Ref.
PANI-GA-0.1S	O_2-sat H_2SO_4 (0.5 M)	2.1	0.6-1.1 V (100 mV/s) 5000 cycles	0.83	This work
3D-N-graphene foam	O_2-sat $HClO_4$ (0.1 M)	0.644	0.6-1.0 V (50 mV/s) 5000 cycles	0.209	[42]
Fe-N_x/rGO	O_2-sat H_2SO_4 (0.5 M)	0.35	0-1.0 V (10 mV/s) 1000 cycles	0.23	[43]

CONCLUSION

Graphene aerogel (GA)-based carbon catalysts were developed for the ORR in the acidic condition. The GA was formed by a simple hydrothermal treatment of graphene oxide dispersion in an aqueous phase. Polyaniline (PANI) was synthesized in the presence of the GA powder. The pyrolysis of PANI-GA at high temperatures of 800-1,000 °C produced N, S-doped carbon catalysts. The proper amount of the catalyst loading on the electrode and the proper concentration of the catalyst ink were found. The thick catalyst layer would cause O_2 or H_2O_2 to reside inside the layer longer, with even higher diffusion-limiting current density than a commercial Pt/C. $FeSO_4$ was added as an auxiliary S source in addition to APS, which was used as an initiator for PANI polymerization. PANI-GA-0.1S sample, which was pyrolyzed at 900 °C, showed the highest mass activity of 2.1 mA/mg at 0.8 V for the ORR in 0.5 M H_2SO_4 solution. The mass activity decreased to 0.83 mA/mg after the ADT, which was performed by repeating CV in a range of 0.6-1.1 V 5000 cycles. The PANI-GA-based carbon catalysts showed good activity and durability compared to other carbon catalysts reported in the literature.

ACKNOWLEDGEMENTS

This work was financially supported by the Global Frontier R&D Program at the Center for Multiscale Energy System (2011-0031575) and NRF-2015R1A2A2A01004467 through the National Research Foundation of Korea funded by the Ministry of Education, Science and Technology.

REFERENCES

1. A. Damjanovic, M. A. Genshaw and J. O. M. Bockris, *J. Chem. Phys.*, **45**, 4057 (1966).
2. B. Wang, *J. Power Sources*, **152**, 1 (2005).
3. R. Jasinski, *Nature*, **201**, 1212 (1964).
4. M. Lefevre, E. Proietti, F. Jaouen and J. P. Dodelet, *Science*, **324**, 71 (2009).
5. H. W. Liang, W. Wei, Z. S. Wu, X. L. Feng and K. Mullen, *J. Am. Chem. Soc.*, **135**, 16002 (2013).
6. G. Wu, K. L. More, C. M. Johnston and P. Zelenay, *Science*, **332**, 443 (2011).
7. S. Kattel, P. Atanassov and B. Kiefer, *Phys. Chem. Chem. Phys.*, **15**, 148 (2013).
8. B. Jeong, D. Shin, H. Jeon, J. D. Ocon, B. S. Mun, J. Baik, H. J. Shin and J. Lee, *ChemSusChem*, **7**, 1289 (2014).
9. S. Yasuda, L. Yu, J. Kim and K. Murakoshi, *Chem. Commun.*, **49**, 9627 (2013).
10. W. P. Ouyang, D. R. Zeng, X. Yu, F. Y. Xie, W. H. Zhang, J. Chen, J. Yan, F. J. Xie, L. Wang, H. Meng and D. S. Yuan, *Int. J. Hydrogen Energy*, **39**, 15996 (2014).
11. U. Tylus, Q. Y. Jia, K. Strickland, N. Ramaswamy, A. Serov, P. Atanassov and S. Mukerjee, *J. Phys. Chem. C*, **118**, 8999 (2014).
12. A. Zitolo, V. Goellner, V. Armel, M. T. Sougrati, T. Mineva, L. Stievano, E. Fonda and F. Jaouen, *Nat. Mater.*, **14**, 937 (2015).
13. A. Muthukrishnan, Y. Nabae, T. Okajima and T. Ohsaka, *ACS Catal.*, **5**, 5194 (2015).
14. Y. G. Li, W. Zhou, H. L. Wang, L. M. Xie, Y. Y. Liang, F. Wei, J. C. Idrobo, S. J. Pennycook and H. J. Dai, *Nat. Nanotechnol.*, **7**, 394 (2012).
15. J. Y. Cheon, T. Kim, Y. Choi, H. Y. Jeong, M. G. Kim, Y. J. Sa, J. Kim, Z. Lee, T. H. Yang, K. Kwon, O. Terasaki, G. G. Park, R. R. Adzic and S. H. Joo, *Sci. Rep.*, **3** (2013).
16. L. T. Le, M. H. Ervin, H. W. Qiu, B. E. Fuchs and W. Y. Lee, *Electrochem. Commun.*, **13**, 355 (2011).
17. M. D. Stoller, S. J. Park, Y. W. Zhu, J. H. An and R. S. Ruoff, *Nano Lett.*, **8**, 3498 (2008).
18. D. W. Wang, Y. G. Min, Y. H. Yu and B. Peng, *J. Colloid Interface Sci.*, **417**, 270 (2014).
19. M. H. Liang and L. J. Zhi, *J. Mater. Chem.*, **19**, 5871 (2009).
20. M. Pumera, *Energy Environ. Sci.*, **4**, 668 (2011).
21. C. H. Lu, H. H. Yang, C. L. Zhu, X. Chen and G. N. Chen, *Angew. Chem. Int. Ed.*, **48**, 4785 (2009).
22. F. Schedin, A. K. Geim, S. V. Morozov, E. W. Hill, P. Blake, M. I. Katsnelson and K. S. Novoselov, *Nat. Mater.*, **6**, 652 (2007).
23. H. W. Hu, J. H. Xin, H. Hu, X. W. Wang and Y. Y. Kong, *Appl. Catal. A*, **492**, 1 (2015).
24. Y. C. Si and E. T. Samulski, *Chem. Mater.*, **20**, 6792 (2008).
25. J. Yan, T. Wei, B. Shao, F. Q. Ma, Z. J. Fan, M. L. Zhang, C. Zheng, Y. C. Shang, W. Z. Qian and F. Wei, *Carbon*, **48**, 1731 (2010).
26. M. W. Chung, C. H. Choi, S. Y. Lee and S. I. Woo, *Nano Energy*, **11**, 526 (2015).
27. C. Li and G. Q. Shi, *Adv. Mater.*, **26**, 3992 (2014).
28. L. L. Jiang and Z. J. Fan, *Nanoscale*, **6**, 1922 (2014).
29. S. Han, D. Q. Wu, S. Li, F. Zhang and X. L. Feng, *Adv. Mater.*, **26**, 849 (2014).
30. C. Li and G. Q. Shi, *Nanoscale*, **4**, 5549 (2012).
31. V. Chabot, D. Higgins, A. P. Yu, X. C. Xiao, Z. W. Chen and J. J. Zhang, *Energy Environ. Sci.*, **7**, 1564 (2014).
32. X. D. Huang, K. Qian, J. Yang, J. Zhang, L. Li, C. Z. Yu and D. Y. Zhao, *Adv. Mater.*, **24**, 4419 (2012).
33. Y. X. Xu, K. X. Sheng, C. Li and G. Q. Shi, *ACS Nano*, **4**, 4324 (2010).
34. D. Ghosh, S. Giri, A. Mandal and C. K. Das, *Appl. Surf. Sci.*, **276**, 120 (2013).
35. C. M. S. Izumi, V. R. L. Constantino, A. M. C. Ferreira and M. L. A. Temperini, *Synth. Met.*, **156**, 654 (2006).
36. G. Wu, C. Zhongwei, A. Kateryna, H. G. Fernando and P. Zelenay, *ECS Trans.*, **16**, 159 (2008).
37. D. C. Marcano, D. V. Kosynkin, J. M. Berlin, A. Sinitskii, Z. Z. Sun, A. Slesarev, L. B. Alemany, W. Lu and J. M. Tour, *ACS Nano*, **4**, 4806 (2010).
38. C. H. Choi, H. K. Lim, M. W. Chung, J. C. Park, H. Shin, H. Kim and S. I. Woo, *J. Am. Chem. Soc.*, **136**, 9070 (2014).
39. J. Liang, Y. Jiao, M. Jaroniec and S. Z. Qiao, *Angew. Chem. Int. Ed.*, **51**, 11496 (2012).
40. L. P. Zhang and Z. H. Xia, *J. Phys. Chem. C*, **115**, 11170 (2011).
41. C. H. Choi, C. Baldizzone, J. P. Grote, A. K. Schuppert, F. Jaouen and K. J. J. Mayrhofer, *Angew. Chem. Int. Ed.*, **54**, 12753 (2015).
42. X. J. Zhou, Z. Y. Bai, M. J. Wu, J. L. Qiao and Z. W. Chen, *J. Mater. Chem. A*, **3**, 3343 (2015).
43. A. H. A. M. Videla, S. Ban, S. Specchia, L. Zhang and J. J. Zhang, *Carbon*, **76**, 386 (2014).